

# Constraint violation in free evolution schemes: comparing BSSNOK with a conformal decomposition of Z4

Sebastiano Bernuzzi and David Hilditch

*Theoretical Physics Institute, University of Jena, 07743 Jena, Germany*

(Dated: May 31, 2019)

We compare numerical evolutions performed with the BSSNOK formulation and a conformal decomposition of a Z4-like formulation of General Relativity. The important difference between the two formulations is that the Z4 formulation has a propagating Hamiltonian constraint, whereas BSSNOK has a zero-speed characteristic variable in the constraint subsystem. In spherical symmetry we evolve both puncture and neutron star initial data. We demonstrate that the propagating nature of the Z4 constraints leads to results that compare favorably with BSSNOK evolutions, especially when matter is present in the spacetime. From the point of view of implementation the new system is a simple modification of BSSNOK.

## I. INTRODUCTION

Numerical evolutions of the Einstein equations are complicated by the constraints of the system. At the continuum level the constraint subsystem of a given formulation of General Relativity (GR) must close; if the constraints are satisfied in one time-slice, they will remain so. There are two possible numerical approaches to the constraints of the system. The first is to perform a so-called constrained evolution, in which the constraints are explicitly resolved at every point in time. There has been some progress in this direction in 3-D numerical relativity since the work of Bonazzola et al. [7] (see also [8, 9] for mathematical analysis and recent developments), but the fact that the constraint equations are elliptic in character is a limitation from the point of view of computational cost. The second, more common approach is to perform a free evolution. For free evolution the constraints are explicitly solved only in the initial time-slice. Throughout an evolution the constraints will be violated by numerical error, but this error should converge away with resolution. Computational resources are however always limited and in some situations a large constraint violation can be responsible for a numerical evolution to fail. Empirically spacetimes which contain matter are especially likely to suffer from large constraint violation.

A major research topic has been the development of methods to minimise constraint violation at finite resolution. An obvious example is the PDEs and numerical analysis of the constraint subsystem of a given formulation. Formulations with a constraint system whose characteristic speeds are non-zero are preferable, since one may hope that constraint violations propagate out of the numerical domain as opposed to sitting on the grid and growing. A related issue is the construction of constraint preserving boundary conditions, which prevent large constraint violations from propagating in from the outer boundary of the computational domain. Here we consider the effect of propagating constraints in combination with a damping scheme.

The idea behind the constraint damping method is to identify places in the main system to subtract con-

straints, such that the implied constraint subsystem picks up terms that force a reduction in the size of any violation. In fact the constraint damping scheme of Gundlach et al. [3] was used in the first successful numerical simulation of the binary black hole merger to dramatic effect. Essentially the same scheme is now used in the state of the art pseudo-spectral code of the Caltech-Cornell collaboration, see for example [30] and in the finite difference codes [10, 31]. All of these successful uses of constraint damping have been for the generalized harmonic formulation of the Einstein equations, which implicitly relies on gauge conditions that are in the principal part harmonic.

On the other hand, many groups have been using the BSSNOK formulation (hereafter BSSN for brevity) with the 1+log and  $\tilde{\Gamma}$ -driver gauge conditions to perform simulations of both matter and vacuum space-times, following the approach of [32, 33]. Unfortunately, there has not been a systematic comparison of the constraint violation between the different approaches, but every piece of evidence indicates that the simulations give comparable, compatible results. The differences between the generalized harmonic and puncture approaches prevent the two methods from being straightforwardly interchanged. For example it is not possible to evolve the standard puncture initial data with the generalized harmonic approach. BSSN on the other hand lacks a constraint damping scheme. In this work we demonstrate that it is possible to evolve spacetimes of interest with a conformal decomposition of the Z4 [1, 2] formulation, which we denote Z4c (conformal Z4). Furthermore we show that the constraint damping scheme for Z4 can be applied effectively and straightforwardly to the modified system. We find the new system particularly efficient in the evolution of non-vacuum spacetimes. From the implementation point of view, the new system is a simple adjustment of the BSSN equations.

In section II the Z4c system is described in some detail. Section III contains a brief review of the equations of relativistic hydrodynamics. Our numerical results are contained in section IV. Finally we conclude in section V.

Through the paper we use geometrical units, numerical results are reported with dimensionless units  $c = G =$

$$M_{\odot} = M_{\text{bh}} = 1.$$

## II. THE Z4C SYSTEM

*Formulation:* The (constraint damped) Z4 formulation [1, 2, 3] takes the 4-dimensional Einstein equations and replaces them by

$$R_{ab} + \nabla_a Z_b + \nabla_b Z_a = 8\pi(T_{ab} - \frac{1}{2}g_{ab}T) + \kappa_1[t_a Z_b + t_b Z_a - (1 + \kappa_2)g_{ab}t_c Z^c], \quad (1)$$

where  $Z_a$  is a 4-vector of constraints and  $t^a$  is a time-like vector field. Solutions of Eq. (1) are also valid solutions of the Einstein equations when the constraints  $Z_a$  vanish. From the PDEs point of view, the most important part of the constraint addition is that of the partial derivatives. The *constraint damping* terms with coefficients  $\kappa_i$  are discussed in more detail in the following section. We 3 + 1 decompose the system and discard non-damping non-principal modifications to the ADM equations. This has the undesirable effect of breaking the 4-covariance of the Z4 formulation, but on the other hand we will see that discarding the lower order terms allows the evolution equations to be written very similarly to BSSN. The time-evolution equations are

$$\partial_t \gamma_{ij} = \mathcal{L}_{\beta} \gamma_{ij} - 2\alpha K_{ij}, \quad (2)$$

$$\begin{aligned} \partial_t K_{ij} = & -D_i D_j \alpha + \alpha[R_{ij} - 2K_{ik} K_j^k + K_{ij} K + 2\partial_{(i} Z_{j)}] \\ & + \mathcal{L}_{\beta} K_{ij} + 4\pi\alpha[\gamma_{ij}(S - \rho_{\text{ADM}}) - 2S_{ij}] \\ & - \kappa_1(1 + \kappa_2)\alpha\gamma_{ij}\Theta, \end{aligned} \quad (3)$$

$$\partial_t \Theta = \alpha\left[\frac{1}{2}H + \partial_k Z^k - (2 + \kappa_2)\kappa_1\Theta\right] + \beta^i \Theta_{,i}, \quad (4)$$

$$\partial_t Z_i = \alpha M_i + \alpha \Theta_{,i} - \alpha \kappa_1 Z_i, \quad (5)$$

where  $Z_i$  is just the spatial projection of  $Z_a$  and  $\Theta = -n_a Z^a$ . We stress that these equations of motion are not identical to those of Z4, although they differ only in non-principal terms. The Hamiltonian and momentum constraints are

$$H \equiv R - K_{ij} K^{ij} + K^2 - 16\pi\rho_{\text{ADM}} = 0, \quad (6)$$

$$M^i \equiv D_j(K^{ij} - \gamma^{ij}K) - 8\pi S^i = 0. \quad (7)$$

We adopt the standard notation for the metric variables and decompose the stress-energy tensor as

$$\rho_{\text{ADM}} = n_a n_b T^{ab}, \quad (8)$$

$$S_i = -\gamma_{ia} n_b T^{ab}, \quad (9)$$

$$S_{ij} = \gamma_{ia} \gamma_{jb} T^{ab}. \quad (10)$$

To write the system as similarly as possible as the BSSN formulation we now conformally decompose the variables, or in other words make the change of variables

$$\tilde{\gamma}_{ij} = \gamma^{-\frac{1}{3}} \gamma_{ij}, \quad \chi = \gamma^{-\frac{1}{3}}, \quad (11)$$

$$\hat{K} = \gamma^{ij} K_{ij} - 2\Theta, \quad \tilde{A}_{ij} = \gamma^{-\frac{1}{3}}(K_{ij} - \frac{1}{3}\gamma_{ij}K), \quad (12)$$

and

$$2Z_i = \tilde{\gamma}_{ij} \tilde{\Gamma}^j - \tilde{\gamma}^{jk} \tilde{\gamma}_{ij,k}, \quad (13)$$

The evolution equations are then

$$\partial_t \chi = \frac{2}{3} \chi [\alpha(\hat{K} + 2\Theta) - D_i \beta^i], \quad (14)$$

$$\partial_t \tilde{\gamma}_{ij} = -2\alpha \tilde{A}_{ij} + \beta^k \tilde{\gamma}_{ij,k} + \tilde{\gamma}_{ik} \beta_{,j}^k - \frac{2}{3} \tilde{\gamma}_{ij} \beta_{,k}^k, \quad (15)$$

$$\begin{aligned} \partial_t \hat{K} = & -D^i D_i \alpha + \alpha[\tilde{A}_{ij} \tilde{A}^{ij} + \frac{1}{3}(\hat{K} + 2\Theta)^2] \\ & + 4\pi\alpha[S + \rho_{\text{ADM}}] + \beta^i K_{,i} + \alpha\kappa_1(1 - \kappa_2)\Theta \end{aligned} \quad (16)$$

the trace-free extrinsic curvature evolves with

$$\begin{aligned} \partial_t \tilde{A}_{ij} = & -\chi[-D_i D_j \alpha + \alpha(R_{ij} - 8\pi S_{ij})]^{\text{tf}} \\ & + \alpha[(\hat{K} + 2\Theta)\tilde{A}_{ij} - 2\tilde{A}_{ik} \tilde{A}_{kj}] \\ & + \beta^k \tilde{A}_{ij,k} + \tilde{A}_{ik} \beta_{,j}^k - \frac{2}{3} \tilde{A}_{ij} \beta_{,k}^k \end{aligned} \quad (17)$$

and finally we have

$$\begin{aligned} \partial_t \tilde{\Gamma}^i = & -2\tilde{A}^{ij} \alpha_{,j} + 2\alpha[\tilde{\Gamma}_{jk}^i \tilde{A}^{jk} - 2\tilde{A}^{ij} \ln(\chi)_{,j} \\ & - \frac{2}{3} \tilde{\gamma}^{ij} (\hat{K} + 2\Theta)_{,j} - 8\pi \tilde{\gamma}^{ij} S_{j}] + \tilde{\gamma}^{jk} \beta_{,j}^i \\ & + \frac{1}{3} \tilde{\gamma}^{ij} \beta_{,k}^k + \beta^j \tilde{\Gamma}_{,j}^i - \tilde{\Gamma}_d^j \beta_{,j}^i + \frac{2}{3} \tilde{\Gamma}_d^i \beta_{,j}^j, \end{aligned} \quad (18)$$

where we write  $\tilde{\gamma}^{jk} \tilde{\Gamma}_{jk}^i = \tilde{\Gamma}_d^i$ . The  $\Theta$  variable evolves according to Eq. (4) with the appropriate substitutions Eqns. (22-25). As with BSSN we write, in the  $\partial_t \tilde{A}_{ij}$  equations

$$R_{ij} = R^{\chi}_{ij} + \tilde{R}_{ij}, \quad (19)$$

$$\begin{aligned} \tilde{R}^{\chi}_{ij} = & \frac{1}{2\chi} \tilde{D}_i \tilde{D}_j \chi + \frac{1}{2\chi} \tilde{\gamma}_{ij} \tilde{D}^l \tilde{D}_l \chi \\ & - \frac{1}{4\chi^2} \tilde{D}_i \chi \tilde{D}_j \chi - \frac{3}{4\chi^2} \tilde{\gamma}_{ij} \tilde{D}^l \chi \tilde{D}_l \chi, \end{aligned} \quad (20)$$

$$\begin{aligned} \tilde{R}_{ij} = & -\frac{1}{2} \tilde{\gamma}^{lm} \tilde{\gamma}_{ij,lm} + \tilde{\gamma}_{k(i} \tilde{\Gamma}_{|j)}^k + \tilde{\Gamma}_d^k \tilde{\Gamma}_{(ij)k} + \\ & \tilde{\gamma}^{lm} \left( 2\tilde{\Gamma}_{l(i}^k \tilde{\Gamma}_{j)km} + \tilde{\Gamma}_{im}^k \tilde{\Gamma}_{klj} \right). \end{aligned} \quad (21)$$

The complete set of constraints are, in terms of the evolved variables, given by

$$\Theta, \quad 2Z_i = \tilde{\gamma}_{ij} \tilde{\Gamma}^j - \tilde{\gamma}^{jk} \tilde{\gamma}_{ij,k}, \quad (22)$$

$$H = R - \tilde{A}^{ij} \tilde{A}_{ij} + \frac{2}{3}(\hat{K} + 2\Theta)^2 - 16\pi\rho_{\text{ADM}}, \quad (23)$$

$$\begin{aligned} \tilde{M}^i = & \partial_j \tilde{A}^{ij} + \tilde{\Gamma}_{jk}^i \tilde{A}^{jk} - \frac{2}{3} \tilde{\gamma}^{ij} \partial_j (\hat{K} + 2\Theta) \\ & - \frac{3}{2} \tilde{A}^{ij} (\log \chi)_{,j}, \end{aligned} \quad (24)$$

$$D \equiv \ln(\det \tilde{\gamma}) = 0, \quad T \equiv \tilde{\gamma}^{ij} \tilde{A}_{ij} = 0 \quad (25)$$

The change of variables introduces the algebraic constraints  $D$  and  $T$ . The numerical implementation explicitly imposes these constraints, so the continuum system we evolve is equivalent to Eqns. (2-5). One may obtain BSSN from Z4c by taking  $\Theta \rightarrow 0$  in Eqns. (14-25).

*Hyperbolicity:* Statements about the hyperbolicity of Z4c obviously follow directly from those about Z4 since the two formulations share the same principal part. For completeness we summarize the relevant results here. A first order in time, second order in space system is called strongly hyperbolic if it has a complete set of characteristic variables with real characteristic speeds. The Z4c system is strongly hyperbolic when coupled to the puncture gauge conditions

$$\partial_t \alpha = \beta^i \alpha_{,i} - \alpha^2 \mu_L \hat{K}, \quad (26)$$

$$\partial_t \beta^i = \mu_S \tilde{\Gamma}^i - \eta \beta^i + \beta^j \beta^i_{,j} \quad (27)$$

in which we always choose  $\mu_L = 2/\alpha$  and  $\mu_S = 1$ . To construct the characteristic variables we perform a 2 + 1 decomposition in space and construct the fully second order characteristic variables [28]. Defining

$$\partial_0 = \frac{1}{\alpha} (\partial_t - \beta^i \partial_i), \quad (28)$$

the scalar sector has characteristic variables

$$U_{s \pm \mu_L} = \partial_0 \alpha \pm \sqrt{\mu_L} \alpha_{,s}, \quad (29)$$

$$U_{s \pm 1} = \partial_0 \gamma_{qq} \pm \gamma_{qq,s}, \quad (30)$$

$$U_{s \pm 1}' = \partial_0 \gamma_{ss} \pm \frac{4}{3} \gamma_{ss,s} \pm \frac{1}{3} \gamma_{qq,s} - \frac{2}{\alpha^2 \mu_L} \partial_0 \alpha - \frac{2}{\alpha} \beta_{s,s} \mp \frac{2}{\alpha^2 \mu_S} \beta_{s,s}, \quad (31)$$

$$U_{s \pm \frac{2}{\sqrt{3}} \mu_S} = \partial_0 \beta_s \pm \frac{\sqrt{3}}{2} \sqrt{\mu_S} \beta_{s,s} - \frac{\alpha \mu_S}{6(1 - \mu_S)} (\gamma_{ss,s} \mp \frac{\sqrt{3}}{2} \sqrt{\mu_S} \partial_0 \gamma_{ss}) - \frac{\alpha \mu_S}{6(1 - \mu_S)} (\gamma_{qq,s} \mp \frac{\sqrt{3}}{2} \sqrt{\mu_S} \partial_0 \gamma_{qq}) - \hat{\mu} (\alpha_{,s} - \sqrt{3 \mu_S} (1 + \frac{1 - \mu_L}{3 - 4 \mu_S}) \partial_0 \alpha) \quad (32)$$

with speeds  $\pm(\sqrt{\mu_L}, 1, 1, \sqrt{3 \mu_S}/2)$  respectively, where

$$\hat{\mu} = \frac{\mu_S (3 - 4 \mu_S)}{(3 \mu_L - 4 \mu_S) (1 - \mu_S)}. \quad (33)$$

The vector sector has characteristic variables

$$U_{A \pm \sqrt{\mu_S}} = \partial_0 \beta_A \pm \sqrt{\mu_S} \beta_{A,s}, \quad (34)$$

$$U_{A \pm 1} = \partial_0 \gamma_{sA} \pm \gamma_{sA,s} - \frac{1}{\mu_S \alpha} (\mu_S \beta_{A,s} \pm \partial_0 \beta_A), \quad (35)$$

with speeds  $\pm(\sqrt{\mu_S}, 1)$ . Finally the tensor sector has characteristic variables

$$U_{AB \pm 1} = \partial_0 \gamma_{AB} \pm \gamma_{AB,s}, \quad (36)$$

with speeds  $\pm 1$ . Note that the choice  $\mu_S = 1$  renders some of the characteristic variables singular. In that special case one should analyse the system independently; it is again strongly hyperbolic, but we omit the characteristic variables. Strong hyperbolicity is enough to guarantee well-posedness of the Cauchy problem. For the initial boundary value problem, the stricter notion of symmetric hyperbolicity is desirable. We do not consider it here.

*Constraint subsystem:* The principal part of the Z4c constraint subsystem is given by

$$\partial_0 \Theta \simeq \frac{1}{2} H + \partial_i Z^i, \quad (37)$$

$$\partial_0 Z_i \simeq M_i + \partial_i \Theta, \quad (38)$$

$$\partial_0 H \simeq -2 \partial_i M^i, \quad (39)$$

$$\partial_0 M_i \simeq -\frac{1}{2} \partial_i H + \partial^j \partial_j Z_i - \partial_i \partial^j Z_j. \quad (40)$$

Each of the variables satisfies a fully second order wave equation. The characteristic variables are simply

$$\partial_0 \Theta \pm \Theta_{,s}, \quad \partial_0 Z_i \pm Z_{i,s}, \quad (41)$$

$$\partial_0 H \pm H_{,s}, \quad \partial_0 M_i \pm M_{i,s}, \quad (42)$$

each with speeds  $\pm 1$ . In the numerical experiments that follow the crucial property is the propagating nature of the Z4c subsystem. The constraint damping scheme adds another level of complexity. However, if we linearize the system around flat-space we trivially recover the Z4 constraint system; the analysis of [3] holds immediately. All but constant frequency constraint violating modes are damped.

*Comparison with the BSSN constraint system:* For a complete discussion of the BSSN formulation we suggest [4, 5, 6]. Here we focus only on the BSSN constraint subsystem in order to compare with that of the Z4c system. Assuming that the algebraic constraints are satisfied, the principal part of the constraint system is given by

$$\partial_0 Z_i \simeq M_i, \quad \partial_0 H \simeq -2 \partial_i M^i, \quad (43)$$

$$\partial_0 M_i \simeq \frac{1}{6} \partial_i H + \partial^j \partial_j Z_i + \frac{1}{3} \partial_i \partial^j Z_j. \quad (44)$$

The characteristic variables are

$$C_{s \pm 1} = Z_{s,s} + \frac{1}{8} H \pm \frac{3}{4} M_s, \quad (45)$$

$$C_{s0} = \frac{1}{2} H + Z_{s,s}. \quad (46)$$

with speeds  $(\pm 1, 0)$  in the scalar sector and

$$C_{A \pm 1} = Z_A \pm M_A, \quad (47)$$

with speeds  $\pm 1$  in the vector sector.

There are two important differences between the two constraint subsystems. The first is that BSSN does not accept a natural constraint damping scheme on every constraint. The second is the 0-speed characteristic variable in the BSSN system. In free-evolution numerical applications, some violation of the constraints is inevitable. Since the numerical scheme will inherit properties from the continuum system, one expects errors in the BSSN Hamiltonian constraint to sit on the numerical grid and, potentially, grow. On the other hand one should expect Z4c Hamiltonian constraint violations to propagate. In combination with suitable boundary conditions and the

damping scheme we expect that Z4 Hamiltonian constraint violations will be easier to control than those of BSSN. The conclusions obtained from the above linear PDEs analysis may not carry over to fully non-linear evolutions. Numerical evolutions are required to test their validity.

### III. RELATIVISTIC HYDRODYNAMICS

We assume that the matter is described by a perfect fluid stress-energy tensor:

$$T_{ab} = \rho h u_a u_b + p g_{ab} , \quad (48)$$

where  $\rho$  is the rest-mass density,  $\epsilon$  is the specific internal energy,  $h \equiv 1 + \epsilon + p/\rho$  is the specific enthalpy,  $p$  is the pressure, and  $u^a$  is the 4-velocity ( $u^a u_a = -1$ ) of the fluid. The total energy density is given by  $\epsilon = \rho(1 + \epsilon)$ .

The General Relativistic HydroDynamics equations for the perfect fluid matter (*ideal* GRHD) are the local conservation law for the energy-momentum tensor, the conservation law for the baryon number and the Equation of State (EoS) of the fluid:

$$\nabla_a T^{ab} = 0, \quad (49)$$

$$\nabla_a (\rho u^a) = 0, \quad (50)$$

$$P(\rho, \epsilon) = p . \quad (51)$$

Following [16] we rewrite Eqns. (49-50) in first-order, flux-conservative form:

$$\partial_t \vec{q} + \partial_i \vec{f}^{(i)}(\vec{q}) = \vec{s}(\vec{q}) , \quad (52)$$

by introducing the *conservative* variables:

$$\vec{q} = \sqrt{\gamma} \{ D, S_k, \tau \}, \quad (53)$$

where

$$D = W \rho, \quad (54)$$

$$S_k = W^2 \rho h v_k, \quad (55)$$

$$\tau = (W^2 \rho h - p) - D . \quad (56)$$

The simple physical interpretation of these variables is that they represent the rest-mass density ( $D$ ), the momentum density ( $S_k$ ) and an internal energy ( $\tau = \rho_{\text{ADM}} - D$ ) as viewed by Eulerian observers. Above  $v^i$  is the fluid velocity measured by the Eulerian observer:

$$v^i = \frac{u^i}{W} + \frac{\beta^i}{\alpha} = \frac{1}{\alpha} \left( \frac{u^i}{u^0} + \beta^i \right) , \quad (57)$$

and  $W$  is the Lorentz factor between the fluid frame and the Eulerian observer,  $W = 1/\sqrt{1 - v^2}$ , with  $v^2 = \gamma_{ij} v^i v^j$ . The fluxes in Eq. (52) are:

$$\begin{aligned} \vec{f}^{(i)} = \sqrt{-g} \left\{ D \left( v^i - \frac{\beta^i}{\alpha} \right), \right. \\ S_k \left( v^i - \frac{\beta^i}{\alpha} \right) + p \delta_k^i, \\ \left. \tau \left( v^i - \frac{\beta^i}{\alpha} \right) + p v^i \right\} \end{aligned} \quad (58)$$

while the source terms are:

$$\vec{s} = \sqrt{-g} \{ 0, \quad (59)$$

$$\begin{aligned} T^{ab} (\partial_a g_{ak} - \Gamma_{ab}^\delta g_{\delta k}), \\ \alpha (T^{a0} \partial_a \ln \alpha - T^{ab} \Gamma_{ab}^0) \} \\ = \sqrt{-g} \{ 0, \quad (60) \end{aligned}$$

$$\begin{aligned} T^{00} \left( \frac{1}{2} \beta^i \beta^j \partial_k \gamma_{ij} - \alpha \partial_k \alpha \right) + \\ + T^{0i} \beta^j \partial_k \gamma_{ij} + T_i^0 \partial_k \beta^i + \frac{1}{2} T^{ij} \partial_k \gamma_{ij}, \\ T^{00} (\beta^i \beta^j K_{ij} - \beta^i \partial_i \alpha) + T^{0i} (2\beta^j K_{ij} - \partial_i \alpha) + T^{ij} K_{ij} \} \end{aligned}$$

Above  $g \equiv \det g_{ab} = -\alpha^2 \gamma$ ,  $\gamma \equiv \det \gamma_{ij}$  and Eq. (60) can be obtained using Eq. (2) in a way to eliminate time derivatives. Note that both the fluxes and the source terms depend also on the *primitives* variables  $\vec{w} = \{p, \rho, \epsilon, v^i\}$ , and the source terms do not depend on derivatives of  $T_{ab}$ . The system in Eq. (52) is strongly hyperbolic provided that the EoS is causal (the sound speed is less than the speed of light) [16].

### IV. NUMERICAL RESULTS

We consider the following set of tests in spherical symmetry:

**Flat spacetime** Evolution of constraint violating initial data. This test shows the basic mechanism of constraint propagation and damping at work;

**Puncture spacetime** Evolution of puncture initial data. Z4c can be successfully used for the simulation of black-hole spacetimes with the puncture gauge;

**Stable star** Evolution of a stable compact star. Constraint propagation and damping are particularly useful in the simulation of non-vacuum spacetimes in which zero speed modes related to the Hamiltonian constraint sit on the grid and grow during the evolution;

**Migrating star** Evolution of an unstable star which migrates towards a stable one. The main features of Z4c are demonstrated in this nonlinear, very dynamical scenario;

**Collapsing star** Evolution of an unstable star which collapses to a black hole. This test involves all of the difficulties of a simulation in numerical relativity: matter, nonlinear dynamics, formation of a singularity and black hole evolution.

The tests are also performed with BSSN for comparison. We stress that the differences between the results are convergent features, and with sufficiently high resolution they can be made arbitrarily small. In the presentation

of the results we focus on the differences in the behavior of the Hamiltonian constraint. There is not a significant difference between the dynamics of the momentum and  $Z_i$  constraints of the two formulations. In Z4c evolutions the  $\Theta$  constraint violation is typically of the same order as that of the Hamiltonian constraint.

In each simulation we take for simplicity the constraint damping parameters  $\kappa_2 = 0$  and  $\kappa_1 \equiv k = \{0, 0.02\}$ , for a Z4c undamped/damped respectively. There is no particular justification for the value  $k = 0.02$ . The value was found to be reasonable after the first numerical experiments. More detailed discussion follows. A systematic study of the  $\kappa$ 's is left for future work.

The gauge choice is given by Eq. (26) and Eq. (27), one flavour of the popular puncture gauge [29]. In Eq. (27) we use  $\eta = 2/M_{\text{ADM}}$ ; choices more popular for matter evolutions, e.g.  $\eta = 0.3/M_{\text{ADM}}$  [14], were tested in some cases, but without significant differences.

The equations solved in these tests are obtained by a *faithful* spherical reduction of the 3D Cartesian equations presented in Sec. II. Details are given in Appendix A. Standard numerical methods based on finite-differences were used to solve them. They are described in Appendix B. While in 1D we may afford much higher resolutions than those of 3D simulations, we restrict to values reasonable for 3D mesh-refinement-parallel codes (see for instance Tab. I). All the figures refer to the highest resolution simulations.

Initial stellar models are built using the polytropic EoS (see Eq. (B3)) with adiabatic index  $\Gamma = 2$  and polytropic constant  $K = 100$  widely used in literature, e.g. Ref. [12]. The stable star model has central density  $\rho_c = 1.280 \times 10^{-3}$ , gravitational mass  $M = 1.400$  and circumferential radius  $R = 9.586$  (isotropic coordinate radius  $r_R = 8.126$ ). The unstable model instead has central density  $\rho_c = 7.993 \times 10^{-3}$ , gravitational mass  $M = 1.448$  and circumferential radius  $R = 5.838$  (isotropic coordinate radius  $r_R = 4.268$ ). The EoS employed during the evolution is the ideal gas:

$$P(\rho, \epsilon) = (\Gamma - 1)\rho\epsilon. \quad (61)$$

### A. Flat-space test

We begin by evolving a large constraint violating perturbation on flat-space. The violation is constructed by adding

$$\delta\chi = \exp(-r^2/10) \quad (62)$$

to the  $\chi$  variable. According to section II we should find that the Z4c Hamiltonian constraint will propagate away from the origin, whereas the BSSN Hamiltonian constraint should split into two components, one stationary and one propagating. Fig. (1) demonstrates exactly the expected behavior. The main panel shows the Hamiltonian violation in space at the final simulated time for

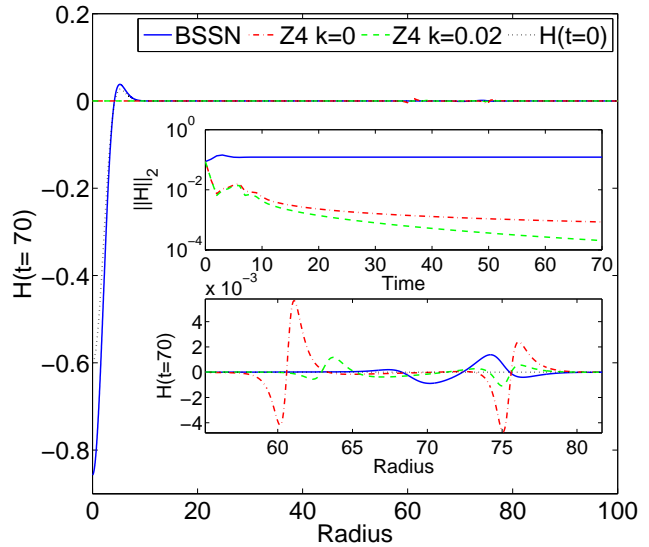


FIG. 1: Hamiltonian constraint violation in the flat spacetime test for BSSN and Z4c. The main panel shows the violation in space at the initial and final time of the simulation. The lower inset focuses on large radii at the final time, where a pulse is propagating outwards (see text for discussion). The upper inset shows the 2-norm of the constraint in time.

the different formulations. In the BSSN evolution the violation near the origin grows (cf. the dotted line, which is  $t = 0$ ), while for the Z4c formulation it has propagated away. The propagation is clear from the lower inset, which shows the violation at large radii; the initial violation propagates out almost completely in a form of a pulse in case of Z4c, and only partially in case of BSSN (the pulse is smaller). Note in addition that the damping mechanism is working effectively in Z4c with  $k = 0.02$ , for which the pulse become progressively smaller in space. Finally in the upper inset the 2-norms are presented. The global behavior of the constraint violation is better for Z4c as time advances.

Note that it is possible to see *over-damping* effects in the Z4c simulations. In fact we experimented with different damping values and for example with  $k = 2$  we found a large constraint-violating “tail” left behind the outgoing pulse near the origin.

The effect of constraint damping has been demonstrated mathematically around flat-space for non-constant in space violations. It is not entirely clear when that analysis will cease to determine the effectiveness of the constraint damping scheme.

### B. Puncture

We evolve a single stationary puncture. Non-trivial evolution occurs due to the gauge adjustment near the puncture. We find little difference in the evolution with

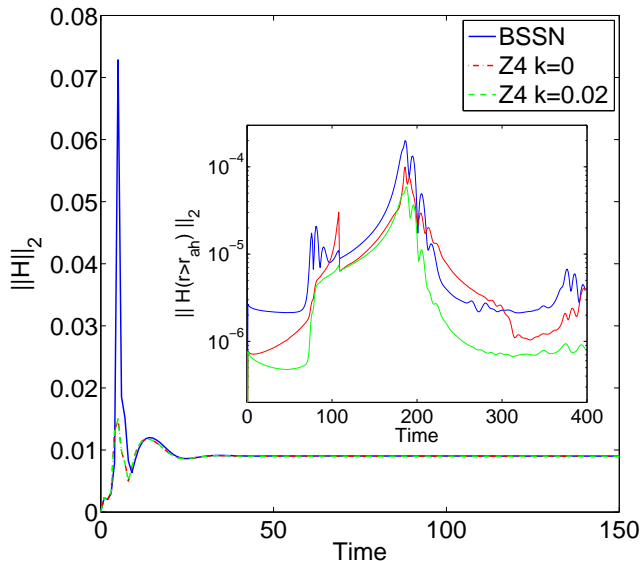


FIG. 2: Hamiltonian constraint violation in the puncture test for BSSN and Z4c. The 2-norm of the constraint is plotted in time. The inset shows the relative difference between the norms of the two simulations.

the two formulations, as well as in violation of the Hamiltonian constraint.

Gauge dynamics dominate the evolution until roughly  $t \sim 25$ . After that the simulations settle at the stationary  $1 + \log$  trumpet solution [26]. Direct comparison with 3D BSSN simulations of the BAM code [27] shows near identical evolution of the metric fields.

The constraint violation results are summarized in Fig. (2) which shows the 2-norm of the Hamiltonian constraint during the evolution. The initial gauge-transient and the stationary phase are clearly recognizable. During the evolution the norm of Z4c is generally slightly better, see for example the inset in Fig. (2) in which the 2-norm computed outside of the horizon is plotted.

Looking at the spatial violation of the Hamiltonian constraint, there is large violation near the puncture, where the numerical solutions are almost identical. The violation is unsurprising since we are finite differencing across an irregular solution. Constraint damping appears to have no effect in a neighborhood of the puncture. Away from the puncture we find that there are small differences in the Hamiltonian constraint violation. All of the simulations in Fig. (2) were performed with Sommerfeld boundary conditions. Incoming constraint violation from the boundary can be seen at  $t = 200$  in the inset of Fig. (2).

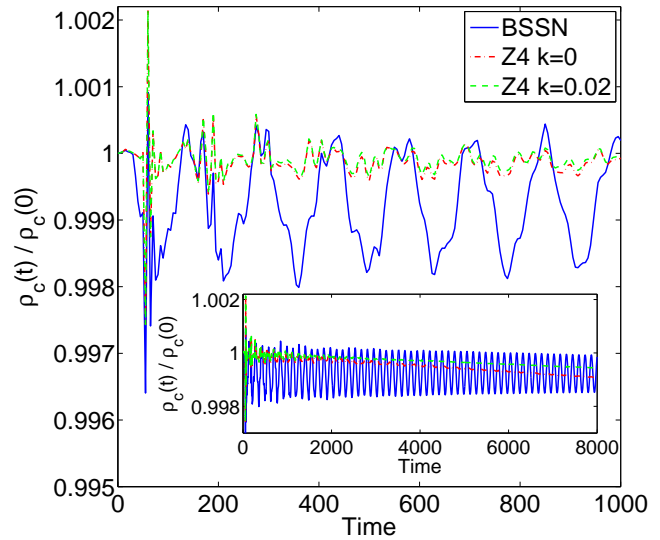


FIG. 3: Oscillations of the central energy density in time in the star test for BSSN and Z4c. The inset shows the same for the whole simulation.

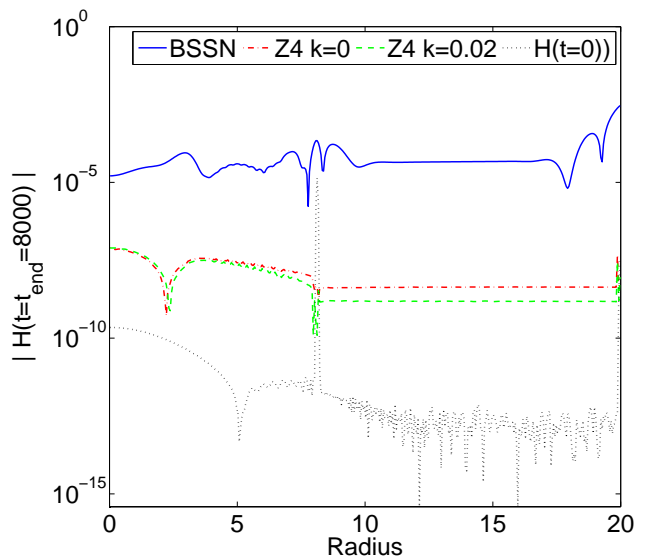


FIG. 4: Hamiltonian constraint violation in the stable star test for BSSN and Z4c. The zero speed mode of the BSSN constraint subsystem causes a slow growth; such growth does not occur in the Z4c evolution. The Z4c constraint damping scheme reduces the size of the violation.

### C. Stable star

We evolve a stable spherical star to  $t_{\text{end}} = 8000$  (around 40 ms). As is standard in such simulations, truncation error causes the star to oscillate at its proper radial frequency. At late times oscillations are eventually

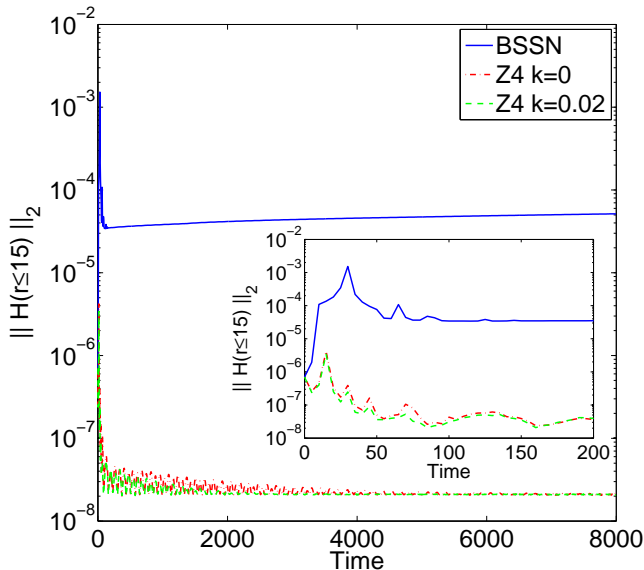


FIG. 5: Hamiltonian constraint violation in the stable star test. The 2-norm of the constraint up to  $r = 15$  is plotted in time. The inset shows a zoom at early times.

damped by the numerical viscosity and by the interaction with the artificial atmosphere; a small linear drift of the mean value is usually also observed, [12, 18]. The numerical error is constraint violating. In this context we expect our linear PDEs analysis to be a good guide to the behavior of the non-linear system, since the unperturbed background solution is static and the numerical error is a small perturbation.

Figure (3) shows the radial oscillations of the central rest-mass density in time. At the same resolution the amplitude of the oscillations in the Z4c evolutions are significantly reduced with respect to BSSN. Additionally at late times they are completely suppressed, as it is clear from the inset, and a drift, which improves in the constrained damped Z4c, can also be seen. The frequencies of the radial mode and its overtones agree in both BSSN and Z4c with the correct values, see e.g. [13] for both perturbative and 3D numerical results.

The dynamics of the Hamiltonian constraint in the BSSN and Z4c evolutions are similar at early times. After the interpolation from our spectral initial data grid to the evolution grid, finite difference derivatives are used to evaluate the Hamiltonian constraint. This produces a relatively large violation in the initial data at the surface of the star. The violation in space at the end of the simulation is plotted in Fig. (4). The dotted line in the figure is the initial violation. In both systems we find that this violation propagates away from the surface of the star. However in the BSSN evolution, the propagation leaves behind a stationary violation that grows linearly in time. This accumulation affect in BSSN is demonstrated in Figs. (4-5).

At the outer boundary a large violation of the constraint is clearly visible in the BSSN evolution. It is caused by the Sommerfeld boundary conditions used with BSSN. This violation is non-convergent but it is usually mitigated by evolving with outer boundary further out, where the Sommerfeld conditions fare much better. The zero speed mode of BSSN plays the important role of keeping this violation at the boundary, thus minimizing their effect on the dynamics. On the other hand we find that for Z4c with Sommerfeld conditions the constraint violation from the outer boundary propagates inside the numerical domain and further perturbs the star, changing for instance the value of the central density and exciting very large amplitude oscillations. The issue is completely solved by the use of maximally dissipative boundary conditions (see Appendix B), which were used in all the matter simulations and in all of the presented figures. One possibility for not finding the same problem in our puncture evolutions is that in that case the constraint violation from the boundary is typically much smaller than the violation at the puncture and so does not significantly alter the dynamics. Also in the black hole evolution we evolve with a much larger outer boundary.

In Fig. (5) we plot the 2-norm of the Hamiltonian constraint in time. The linear growth of the BSSN Hamiltonian constraint is visible when the norm is computed up to  $r \leq 15$  instead of the full grid. The norm on the full grid is in fact dominated by the violation caused by the Sommerfeld boundary conditions (see also again Fig. (4)). The reason is that the violation inside the star converges. At lower resolutions however the linear growth of the Hamiltonian constraint is visible in the norm on the full grid. Note that although Fig. (5) shows that the norm of the Hamiltonian constraint in the Z4c evolution drops below the initial value, the reason is the violation at the surface of the star in the initial data. Fig. (4) shows that pointwise, at the end of the evolution the constraint violation has not dropped below the initial value except in a neighborhood of the surface of the star.

Our experiments indicate that the propagation of the constraints is more helpful in preventing growth than constraint damping.

#### D. Migration

For the migration test we evolve initial data in hydrostatic equilibrium that is unstable against first order perturbations. Truncation error causes the star to migrate to a model in the stable branch of the equilibrium configuration space. The energy difference between the two models is converted into kinetic energy and generates large nonlinear pulsations. With an ideal EoS the transition involves the formation of a shock wave between an inner core and an outer (lower density) mantle which dissipates kinetic energy into thermal energy. Furthermore a small amount of mass is expelled from the star when the shock reaches the surface. The dynamics are



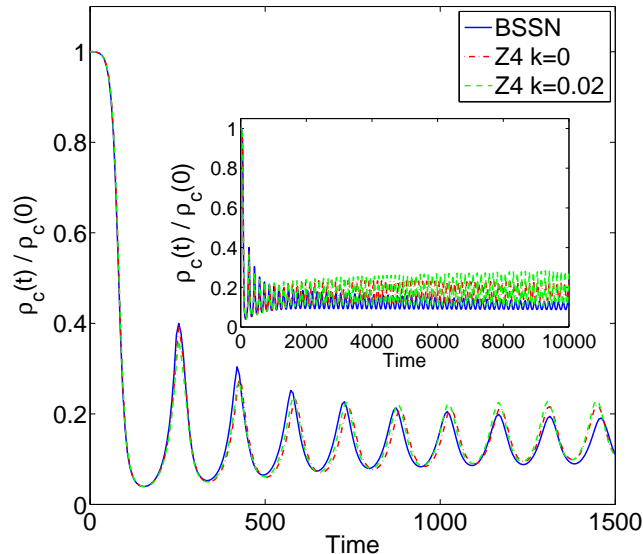


FIG. 6: Oscillations of the central energy density in time in the migration test for BSSN and Z4c.

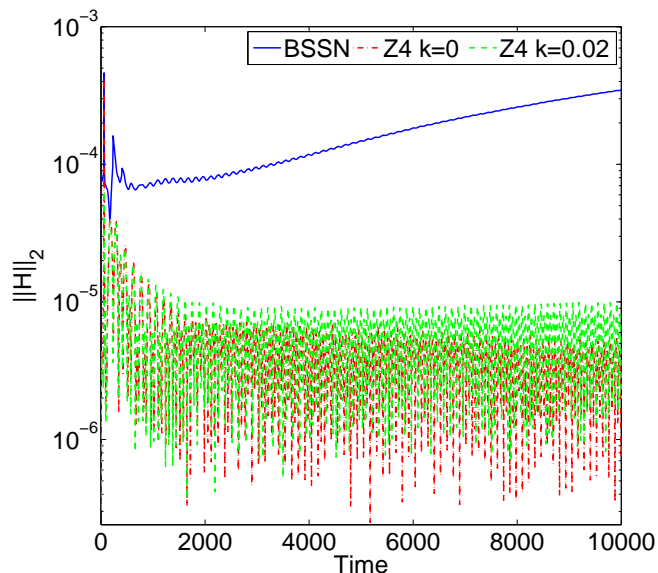


FIG. 7: Hamiltonian constraint violation in the migration test. The 2-norm of the constraint is plotted in time.

described in detail in [9, 12]. This test is important because it probes the behavior of the two formulations in a genuinely non-trivial situation, where the applicability of the linear analysis is unclear.

Figure (6) shows the central density during the simulation: the strong nonlinear oscillations are clearly visible and each is accompanied by a bounce of the core of the star which feeds the shock. At early times the dynamics

are comparable with very small differences. At late times (see the inset) however we find some differences between both BSSN and Z4c both with and without the damping scheme. We believe the simulations at this point are not quantitatively reliable because of the lack of accuracy and convergence, so possible physical differences are not distinguishable from numerical errors.

A second simulation carried with polytropic EoS (see Appendix B, Eq. (B3)), which excludes a priori the presence of shocks [35], completely solves this issue. Even at late times the solutions are comparable and the results obtained with BSSN and Z4c with  $k = 0$  are basically the same. Oscillations in this case are a little damped only by the numerical dissipation. We furthermore observe that the data obtained with Z4c and  $k = 0.02$  are affected by some additional damping.

The Hamiltonian violation behavior is qualitatively the same as in the stable star test. In Fig. (7) the 2-norm is plotted: the linear growth in the BSSN evolution is clearly visible (note that the boundary in this case is further out, so the Sommerfeld boundary condition contributes relatively little to the global violation) while the Z4c evolutions show a propagating and decreasing violation. As opposed to the stable star case, at late times  $t > 2000$  the 2-norm for Z4c damped is larger than Z4c undamped, but this is again a numerical artifact due to the reasons discussed above. The simulations performed with the polytropic EoS result in a behavior analogue to that in Fig. (5).

## E. Collapse

Our final test is the evolution of the unstable star, which we perturb by a small (momentum constraint violating) function

$$\delta v^r = -0.005 \sin\left(\frac{\pi r}{R}\right), \quad (63)$$

to trigger collapse to a black hole. The solution space of the two formulations is not the same when the constraints are not satisfied. However we are able to follow the collapse with both BSSN and Z4c, and do not find significant differences in the dynamics of the two systems. This can be seen for instance in the upper panel of Fig. (8) in which we plot the central lapse in time. During the collapse the rest-mass is conserved to within a 1% error even in our lowest resolution simulation.

The Hamiltonian constraint violation of the formulations as the apparent horizon forms ( $t \simeq 50$ ) is comparable Fig. (9), but afterwards we find once again the linear growth in time of the BSSN Hamiltonian constraint. Finally the lower panel of Fig. (8) shows that after the collapse the irreducible mass of the black hole:

$$M_{\text{irr}} = \sqrt{\frac{A_{\text{ah}}}{16\pi}} \quad (64)$$

where  $A_{\text{ah}}$  is the area evaluated from the apparent horizon, drifts from the correct value by roughly 1% in



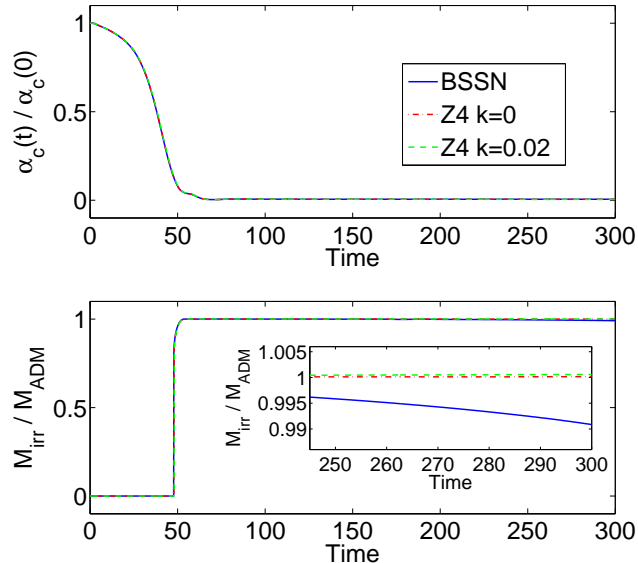


FIG. 8: Collapse dynamics: (upper panel) central value of the lapse and (bottom panel) irreducible mass of the black hole are plotted in time in the collapse test for BSSN and Z4c. The inset in the bottom panel shows a zoom of the irreducible mass at late time.

our BSSN evolution. At our lowest resolution (see Appendix B) this drift is a serious ( $\simeq 25\%$  by  $t = 300$ ) problem, but it converges away at second order. On the other hand, the drift does not occur in any of the Z4c tests. Even at the lowest resolution the Z4c mass drift is below 0.1%. We mention that in Ref. [14], in which a different value of  $\eta$  in the gauge condition is used, this effect is not seen.

## V. CONCLUSION

Despite their success in the evolution of binary black hole and neutron star systems, the solutions of the free-evolution schemes widely used in numerical relativity simulations have some constraint violation. Motivated by the observation that BSSN evolutions of matter spacetimes typically have much larger Hamiltonian than (the almost negligible) momentum constraint violation, we considered the PDE properties of the BSSN constraint subsystem. The constraint subsystem has a zero speed characteristic variable involving the Hamiltonian constraint, which we argue is the cause of the large violation. To demonstrate this with the aim of further improving the formulation for free-evolution schemes, we compare BSSN evolutions with those of a new conformal decomposition of the Z4 formulation. The latter formulation, referred as Z4c, has three desirable properties. Firstly the convenient choice of variables enables the evolution

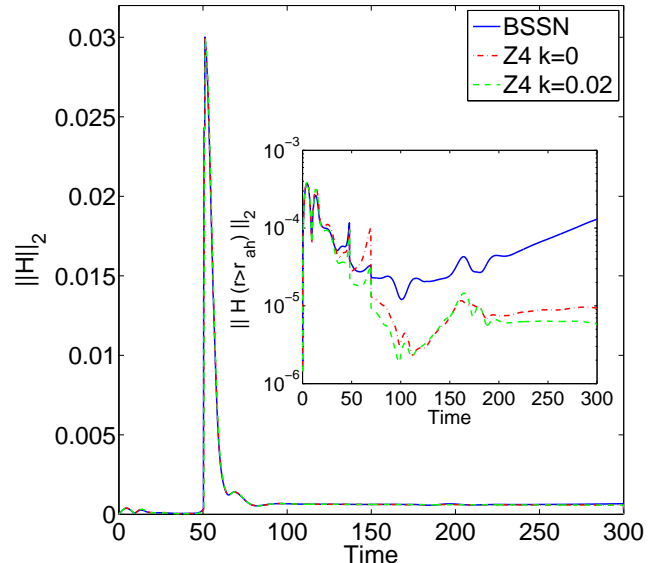


FIG. 9: Hamiltonian constraint violation in the collapse test. The 2-norm of the constraint is plotted in time. The inset shows the 2-norm computed only outside the apparent horizon; notice the log-scale of the y-axis.

of puncture initial data. Secondly it inherits the propagating constraints of undecomposed system. Finally the constraint damping scheme described in [3] can be attached to the new system.

In a large set of tests in spherical symmetry, performed with faithful spherical reductions of the two Cartesian systems, we have demonstrated that the BSSN constraint violation can indeed be avoided by using a system with propagating constraints. We focus on the differences in the Hamiltonian constraint violation because other variables do not show significant differences. We find that the propagation of the constraints is more helpful than the constraint damping scheme in controlling the violation. We also find that when using the Z4c formulation boundary conditions are typically more important than when using BSSN. In our tests we find that maximally dissipative conditions are always sufficient to avoid large constraint violation entering the grid from the outer boundary in Z4c evolutions.

Specifically we perform five tests, and focus on constraint violation. We always find qualitatively the same behavior (similar orders of magnitude) in the momentum constraints of the different systems. Therefore we focus on the behavior of the Hamiltonian constraint. Firstly with a constraint violating perturbation on flat-space we find that the Z4c (BSSN) Hamiltonian constraint does (not) propagate, and that the Z4c constraint damping scheme works. Next we evolve a single puncture and find only small differences in the evolutions. When evolving either a stable or migrating star we find that at typical

resolutions the Z4c Hamiltonian constraint violation is three or four orders of magnitude lower than that with BSSN. The migration test is especially important because it involves long-term nonlinear evolution. Our final test is the evolution of a star collapsing to a black hole. We find that the two formulations give very similar dynamics, which is not guaranteed because our initial data is constraint violating. We find that after the collapse the BSSN Hamiltonian constraint grows linearly in time, and that the irreducible mass of the black hole is not perfectly conserved at low resolutions. These problems are not present in the Z4c tests.

In the work presented here we have not tuned the constraint damping parameters, so an obvious step is to investigate the effect of these parameters in more detail. However the most important follow up is to investigate whether or not similar results can be reproduced in 3D, where there may be additional issues affecting numerical stability. If 3D astrophysical simulations with Z4c are possible it will be interesting to see whether or not the improved Hamiltonian constraint behavior will effect the physics, in particular the extracted gravitational waves from binary systems or stellar collapse.

### Acknowledgments

It is a pleasure to thank Bernd Brügmann, Roman Gold and Pedro Montero for valuable discussions and comments on the manuscript. We also wish to thank Luca Del Zanna, Harry Dimmelmeier, Toni Font and Ian Hawke for helpful advice on HRSC schemes. This work was supported in part by DFG grant SFB/Transregio 7 “Gravitational Wave Astronomy”.

### APPENDIX A: SPHERICAL REDUCTION OF THE EQUATIONS

In spherical symmetry the line-element is:

$$ds^2 = -(\alpha^2 - \beta_r \beta^r) dt^2 + 2\beta_r dr dt + \gamma_{rr} dr^2 + \gamma_T r^2 d\Omega^2, \quad (\text{A1})$$

where  $\beta_r = \beta^r / \gamma_{rr}$ . The determinant of the 3-metric can be written as:

$$\gamma = r^4 \sin^2 \theta \gamma^s, \quad (\text{A2})$$

with the definition  $\gamma^s \equiv \gamma_{rr} \gamma_T^2$ . For the spherical reduction of the metric equations we follow [11]. An auxiliary flat derivative whose connection vanishes in Cartesian coordinates is defined. The standard formulation of the equations of motion is given in Cartesian coordinates. Thus the spherical reduction is made by replacing partial derivatives in constraint addition terms and non-tensorial variables with the auxiliary derivative, and simply rotating from Cartesian to spherical coordinates assuming two angular killing vectors. The resulting expressions are too unwieldy to be presented here.

The spherical reduction of the hydrodynamics equations of motion (52) is performed defining conservative variables as:

$$\vec{q} \equiv \sqrt{\gamma^s} \{D, S_r, \tau\}. \quad (\text{A3})$$

The equations result in a flux-balance form with the fluxes given by:

$$\begin{aligned} \vec{f}^{(r)} &\equiv \alpha \sqrt{\gamma^s} \left\{ D \left( v^r - \frac{\beta^r}{\alpha} \right), \right. \\ &S_r \left( v^r - \frac{\beta^r}{\alpha} \right) + p, \\ &\left. \tau \left( v^r - \frac{\beta^r}{\alpha} \right) + p v^r \right\} \end{aligned} \quad (\text{A4})$$

and source terms by:

$$\begin{aligned} \vec{s} &= \left\{ -\frac{2}{r} f_D^{(r)}, \right. \\ &-\frac{2}{r} f_{S_r}^{(r)} + \alpha \sqrt{\gamma^s} \left( T^{00} \left[ \frac{1}{2} (\beta^r)^2 \partial_r \gamma_{rr} - \alpha \partial_r \alpha \right] + T^{0r} \beta^r \partial_r \gamma_{rr} + T_r^0 \partial_r \beta^r + \frac{1}{2} T^{rr} \partial_r \gamma_{rr} + \frac{p}{\gamma_T} \partial_r \gamma_T \right), \\ &\left. -\frac{2}{r} f_\tau^{(r)} + \alpha \sqrt{\gamma^s} \left( T^{00} \left( (\beta^r)^2 K_{rr} - \beta^r \partial_r \alpha \right) + T^{0r} (2\beta^r K_{rr} - \partial_r \alpha) + T^{rr} K_{rr} + \frac{2pK_T}{\gamma_T} \right) \right\}. \end{aligned} \quad (\text{A5})$$

Note that, as in the field equations, all the source terms

are regular, due to the regularity conditions at the origin,

TABLE I: Settings used in the simulations. Note that dimensionless units  $c = G = M_\odot = M_{\text{bh}} = 1$  are employed.

Test	Resolution, $N$	Grid Atmosphere			Time
	$\{low, med, hig\}$	$r_{\text{out}}$	$f_{\text{thr}}$	$f_{\text{lev}}$	$t_{\text{end}}, c_{\text{eff}}$
Flat	{1000, 2000, 4000}	100	{-, -}		70, 0.5
Puncture	{2000, 4000, 8000}	200	{-, -}		400, 0.5
Stable Star	{100, 200, 400}	20	$10^{-8}, 10^{-12}$		8000, 0.5
Migration	{300, 600, 1200}	40	$10^{-6}, 10^{-9}$		10000, 0.25
Collapse	{400, 800, 1600}	20	$10^{-7}, 10^{-12}$		300, 0.5

since  $1/r$  terms appear always together with a vector quantity. Note also that the system is slightly different from a previous formulation, see e.g. Ref. [19, 20], and in our case the characteristic speeds are the same as the 1D Cartesian one given in [16], once the formal replacements  $\gamma \mapsto \gamma^s$ ,  $v^x \mapsto v^r$  and  $\gamma^{xx} \mapsto \gamma^{rr}$  are applied.

## APPENDIX B: IMPLEMENTATION

Matter and metric fields are integrated forward in time together using the Method of Lines (MoL) based on Runge-Kutta (RK) integrators. Both TVD 3rd-order and 4th-order RK, see e.g. [21], were used for the computations subjected to the Courant condition for the timestep  $\Delta t = c_{\text{eff}} \Delta r$ .

The RHS of the equations are discretized on a staggered grid in  $r \in (0, r_{\text{out}}]$  with uniform spacing  $\Delta r = r_{\text{out}}/N$ . Spatial derivatives of the geometric fields are discretized using centered 4th-order finite differences, and the 4th-order Kreiss-Oliger dissipation operator is used in simulations to stabilize the origin (in Cartesian coordinates it may not be needed for matter simulations) with  $\sigma = 0.007$ . All the relevant parameters used are listed in Tab. I.

We use two different boundary conditions on the metric variables; Sommerfeld and maximally dissipative. With BSSN we always use Sommerfeld conditions like those typically used in 3D implementations. At the boundary each variable is modeled by flat space plus a perturbation. One may then derive the boundary conditions

$$\partial_t f = -v f_{,r} - \frac{v}{r}(f - f_0), \quad (\text{B1})$$

where  $f_0$  is the background solution of the field. For Z4 we also use maximally dissipative boundary conditions. To construct the conditions we linearize the spherical equations of motion around flat-space and analyze the system in fully second order form. We construct the incoming characteristic variables and use conditions

$$U_- = g. \quad (\text{B2})$$

The given data  $g$  for the boundary conditions is taken from the initial data and held constant. The fully second order characteristic variables always contain terms like  $\partial_0 f$  for the evolved variables, and may be solved for evolution equations for  $(\alpha, \beta^r, \chi, \tilde{\gamma}_{rr}, \tilde{\gamma}_T)$  at the boundary if one additionally adds the  $D$  constraint to the boundary conditions. We could use the same method to derive constraint preserving conditions, but for now we find that the maximally dissipative conditions are satisfactory. At typical resolutions we find that the incoming constraint violation is of the order  $10^{-7} - 10^{-8}$  (see Fig. (4)).

Hydrodynamics equations are solved with an High-Resolution-Shock-Capturing (HRSC) method based on cell-center discretization and on the Local-Lax-Friedrichs (LLF) central scheme for the fluxes. The method is described in [23, 24] and we refer the reader to these references for all of the details. The assessment of the LLF flux in case of neutron star evolutions in full GR is presented in [25]. Different reconstruction schemes were tested, overall: the linear TVD based on Van-Leer Monotonized Centered limiter (MC2), the Convex-Essentially-Non-Oscillatory 3rd-order method (CENO3) and the Piecewise Parabolic Method (PPM). No relevant differences were found and the data presented were obtained with the CENO3 reconstruction. The metric fields are reconstructed with either simple averages or *upwinded* Lagrangian quartic reconstruction.

The vacuum treatment is done with the use of an artificial atmosphere as described in [22]. When, during the recovery of primitive variables, a point finish below a certain threshold  $\rho_{\text{thr}} = f_{\text{thr}} \max(\rho(t=0))$  all the variables are set to the atmosphere level  $\rho_{\text{lev}} = f_{\text{lev}} \max(\rho(t=0)) < \rho_{\text{thr}}$ . Typical values are listed in Tab. I.

In the collapse simulations matter fields were set to the atmosphere value once the horizon is formed and if  $\alpha < \alpha_{\text{hydro-ex}} = 0.02$ . This is necessary to avoid numerical problems with the first points close to the origin.

The code has been extensively tested for different problems, especially the HRSC scheme. As expected, 4th order accuracy is reached in vacuum, while matter simulations are accurate at 2nd order (except for situation with shocks).

Stellar initial data are computed with a 2-domain pseudo-spectral method to solve the equations of Ref. [15] in isotropic coordinates, in spherical symmetry. A  $\Gamma = 2$  polytropic EoS:

$$P(\rho) = (\Gamma - 1)\rho\epsilon \quad \text{with} \quad \epsilon = K \frac{\rho^{\Gamma-1}}{\Gamma - 1} \quad (\text{B3})$$

is used with  $K = 100$  which is compatible with the ideal gas EoS used for the evolution. Chebyshev-Gauss-Lobatto grids with 64 collocation points per domain are sufficient for having the equations satisfied to machine accuracy.

- 
- [1] C. Bona, T. Ledvinka, C. Palenzuela and M. Zacek, Phys. Rev. D **67**, 104005 (2003) [arXiv:gr-qc/0302083].
- [2] C. Bona and C. Palenzuela, Phys. Rev. D **69**, 104003 (2004) [arXiv:gr-qc/0401019].
- [3] C. Gundlach, J. M. Martin-Garcia, G. Calabrese and I. Hinder, Class. Quant. Grav. **22** (2005) 3767 [arXiv:gr-qc/0504114].
- [4] T. W. Baumgarte and S. L. Shapiro, Phys. Rept. **376** (2003) 41 [arXiv:gr-qc/0211028].
- [5] E.ourgoulhon, arXiv:gr-qc/0703035.
- [6] M. Alcubierre Oxford University Press (2008).
- [7] S. Bonazzola, E.ourgoulhon, P. Grandclement and J. Novak, Phys. Rev. D **70** (2004) 104007 [arXiv:gr-qc/0307082].
- [8] I. Cordero-Carrion, J. M. Ibanez, E.ourgoulhon, J. L. Jaramillo and J. Novak, Phys. Rev. D **77** (2008) 084007 [arXiv:0802.3018 [gr-qc]].
- [9] I. Cordero-Carrion, P. Cerda-Duran, H. Dimmelmeier, J. L. Jaramillo, J. Novak and E.ourgoulhon, Phys. Rev. D **79** (2009) 024017 [arXiv:0809.2325 [gr-qc]].
- [10] B. Szilagyi, D. Pollney, L. Rezzolla, J. Thornburg and J. Winicour, Class. Quant. Grav. **24** (2007) S275 [arXiv:gr-qc/0612150].
- [11] D. Garfinkle, C. Gundlach and D. Hilditch, Class. Quant. Grav. **25** (2008) 075007 [arXiv:0707.0726 [gr-qc]].
- [12] J. A. Font *et al.*, Phys. Rev. D **65** (2002) 084024 [arXiv:gr-qc/0110047].
- [13] L. Baiotti, S. Bernuzzi, G. Corvino, R. De Pietri and A. Nagar, Phys. Rev. D **79** (2009) 024002 [arXiv:0808.4002 [gr-qc]].
- [14] P. J. Montero, J. A. Font and M. Shibata, Phys. Rev. D **78** (2008) 064037 [arXiv:0805.3099 [gr-qc]].
- [15] S. Bonazzola, E.ourgoulhon, M. Salgado and A. J. Marck, Astron. Astrophys. **278** (1993) 421-443.
- [16] F. Banyuls, J. A. Font, and J. M. A. Ibanez, and J. M. A. Marti, and J. A. Miralles, Astrophys. J. **476** (1997) 221.
- [17] J. A. Font, Living Rev. Rel. **11** (2007) 7.
- [18] J. A. Font, N. Stergioulas and K. D. Kokkotas, Mon. Not. Roy. Astron. Soc. **313** (2000) 678 [arXiv:gr-qc/9908010].
- [19] E.ourgoulhon, Astron. Astrophys. **252** (1991) 651.
- [20] J. V. Romero, J. M. Ibanez, J. M. Marti and J. A. Miralles, Astrophys. J. **462** (1996) 839. [arXiv:astro-ph/9509121].
- [21] C. W. Shu, and S. Osher, J. Comput. Phys. **77** (1988) 439.
- [22] H. Dimmelmeier, J. A. Font and E. Müller, Astron. Astrophys. **388** (2002) 917 [arXiv:astro-ph/0204288].
- [23] L. D. Zanna and N. Bucciantini, Astron. Astrophys. **390** (2002) 1177 [arXiv:astro-ph/0205290].
- [24] L. Del Zanna, O. Zanotti, N. Bucciantini and P. Londrillo, Astron. Astrophys. **473** (2007) 11 [arXiv:0704.3206 [astro-ph]].
- [25] M. Shibata and J. A. Font, Phys. Rev. D **72** (2005) 047501 [arXiv:gr-qc/0507099].
- [26] M. Hannam, S. Husa, D. Pollney, B. Brügmann and N. O'Murchadha, Phys. Rev. Lett. **99** (2007) 241102 [arXiv:gr-qc/0606099].
- [27] B. Brügmann, J. A. Gonzalez, M. Hannam, S. Husa, U. Sperhake and W. Tichy, Phys. Rev. D **77** (2008) 024027 [arXiv:gr-qc/0610128].
- [28] David Hilditch and Ronny Richter, *In Preparation*
- [29] J. R. van Meter, J. G. Baker, M. Koppitz and D. I. Choi, Phys. Rev. D **73** (2006) 124011 [arXiv:gr-qc/0605030].
- [30] M. A. Scheel, M. Boyle, T. Chu, L. E. Kidder, K. D. Matthews and H. P. Pfeiffer, Phys. Rev. D **79** (2009) 024003 [arXiv:0810.1767 [gr-qc]].
- [31] C. Palenzuela, M. Anderson, L. Lehner, S. L. Liebling and D. Neilsen, Phys. Rev. Lett. **103** (2009) 081101 [arXiv:0905.1121 [astro-ph.HE]].
- [32] J. G. Baker, J. Centrella, D. I. Choi, M. Koppitz and J. van Meter, Phys. Rev. Lett. **96** (2006) 111102 [arXiv:gr-qc/0511103].
- [33] M. Campanelli, C. O. Lousto, P. Marronetti and Y. Zlochower, Phys. Rev. Lett. **96** (2006) 111101 [arXiv:gr-qc/0511048].
- [34] F. Herrmann, D. Shoemaker and P. Laguna, arXiv:gr-qc/0601026.
- [35] Another difference when a one parameter EoS  $P(\rho, \epsilon) = P(\rho)$  is used is that the GRHD equation for  $\tau$  is equivalent to the equation for  $D$  and thus need not be evolved.